



Effect of metal oxide contents on the structure and performance of spray-dried CrVO₄/SiO₂ catalysts for the ammoxidation of chlorotoluenes



Jiale Tong¹ · Yeyin Huang¹ · Wanjun Tang¹ · Qingliang You² · Guangyong Xie¹

Received: 6 May 2024 / Accepted: 25 June 2024 / Published online: 29 June 2024
© The Author(s), under exclusive licence to Springer Nature B.V. 2024

Abstract

This work aims at developing a customized ammoxidation catalyst through optimizing the metal oxide content in CrVO₄/SiO₂ catalysts. Various amounts of Cr–V–O with 1:1 molar ratio of Cr/V were successfully loaded on SiO₂ via spray-drying method with colloidal silica as the binder. Polarized light microscope illustrated that the CrVO₄/SiO₂ particles presented as well dispersed microspheres in the microsize (20–80 μm). X-ray diffraction spectra confirmed the formation of monoclinic CrVO₄ phase wherein the metal oxide content was ranged from 30 to 70 weight percent. FT-IR spectra indicated that the introduction of metal oxide had no obvious effects on the skeletal structure of SiO₂. X-ray photoelectron spectroscopy analysis revealed that the valence state of V and Cr was hardly affected with increasing the metal oxide content. Performances of the obtained CrVO₄/SiO₂ catalysts with different metal oxide contents were investigated via the ammoxidation of a model compound, namely para-chlorotoluene (PCT) to para-chlorobenzonitrile (PCBN). A maximum conversion of 99.6% of PCT and 86.5% yield and 86.8% selectivity to PCBN have been obtained over the CrVO₄/SiO₂ catalyst with 60% weight of metal oxides at a temperature of 410 °C, $n(\text{PCT}):n(\text{NH}_3):n(\text{air})=1:3:15$ and reaction load=0.13 g/gCat·h. In addition, this catalyst was efficient and selective toward ammoxidation reactions of toluene, ortho- and meta-chlorotoluenes.

Graphical abstract

$V_2O_5+CrO_3$ +Oxalic acid +(1-v)Colloidal silica	Reaction Conditions		Phases	Catalytic Performance
0.2			Monoclinic $CrVO_4$ + hexagonal- Cr_2O_3	Low
0.3–0.5			Monoclinic $CrVO_4$	Medium
0.6			Monoclinic $CrVO_4$	High
0.7			Monoclinic $CrVO_4$	Medium
1			Orthorhombic $CrVO_4$	Medium
	180°C	300°C/2h →550°C/4h		

Keywords Heterogeneous catalyst · Ammoxidation · Monoclinic $CrVO_4$ · Spray-drying method

Introduction

Chloro-substituted benzonitriles are important chemical intermediates for the synthesis of various value-added chemicals such as herbicides [1], pesticides, pharmaceuticals [2], and so on. The preparation of these benzonitriles via a catalytic ammoxidation process is of particular interest [3]. Vanadium oxides (VO_x) are efficient catalysts for ammoxidation reactions due to their redox property and acidity, and VO_x based catalysts have been widely used in research and industry [4]. Usually, the performance of VO_x catalysts can be improved by adding other components (e.g., P, Cr, Ti, Mo, or Sb) and various mixed oxide ammoxidation catalysts have been designed [5–15]. It is usually accepted that the ammoxidation reaction follows a bifunctional catalysis mechanism [16], of which requires redox and acidic sites simultaneously. Cr can act as an effective promoter and V–Cr–O based composite oxides are known to be highly efficient catalysts for selective gas-phase ammoxidation of chloro-substituted toluenes. Our group focuses on developing V–Cr–O composite oxide catalysts with high activity of ammoxidation reactions [8–10]. Nano- or microsized V–Cr–O catalysts have been prepared by several methods such as solid-state reaction [5], co-precipitation [6], hydrothermal [7–9], and solvothermal routes [10]. It was found that monoclinic $CrVO_4$ had higher catalytic activity than orthorhombic $CrVO_4$, monoclinic $Cr_2V_4O_{13}$, and Cr_2O_3 – V_2O_5 mixed oxides [8]. However, high-cost and low-strength restricted their use in fluid-bed reactors. Supported V–Cr–O catalysts usually have better catalytic activity than unsupported ones due to controllable catalyst textures, large surface area, high mechanical strength, and heat transfer capacity. Supported catalysts were usually prepared via a wetness impregnation process. Active components were dispersed on the surface of carrier. However, the surface of catalyst could be severely worn and teared in a fluidized bed reactor, resulting in a rapid inactivation. Spray-drying method has the

characteristics of fast heat transfer, large evaporation rate, short drying time, and low equipment cost [17]. Comparing with the impregnation method, the spray-drying process is known to be simple, low cost, reliable, and easy to control the particle size and morphology [18–21]. During the spray-drying process, binders such as silica and alumina sols played a role in cross-linking among catalyst particles. The developed catalysts exhibited a fluidizable microspherical shape and strong mechanical strength [22, 23]. In addition, the type and content of inorganic binders were essential in determining the inner structure of catalysts, which directly affected the catalytic performance. As supported catalysts were fabricated using spray-drying method, active components were dispersed on the surface and inner of carriers [24, 25]. Surface wear and tear exposed inner active components and the catalytic activity remained. Very recently, silica supported V–Cr–O catalyst reported by us was prepared via spray drying [26]. It was found that 1:1 molar ratio of Cr/V resulted in the formation of monoclinic CrVO_4 phase, which exhibited the best catalytic performance for ammoxidation of para-chlorotoluene. In this process, silica binder was also used as a support material, helping to increase the catalyst's mechanical strength, to maintain the chemical and physical stability, and to lower production cost. However, the structural aspects of supported monoclinic CrVO_4 catalysts with different silica dosages were not reported. Meanwhile, the effect of silica dosage on the catalytic behavior of $\text{CrVO}_4/\text{SiO}_2$ catalysts was imperceptible. Increasing the silica dosage could modify the surface structure [27, 28], change heat and oxygen transfer capacity [29], and lessen the content of active metal oxides. Therefore, a systematic investigation should be processed to optimize the silica dosage for better catalytic performance.

In the present work, $\text{CrVO}_4/\text{SiO}_2$ catalysts with different metal oxide contents were prepared via spray-drying method. The catalysts were characterized by X-ray diffraction (XRD), polarized light microscope (PLM), X-ray photoelectron spectroscopy (XPS), and hydrogen temperature programmed reduction (H_2 -TPR). In addition, the activities of the spray-dried $\text{CrVO}_4/\text{SiO}_2$ catalysts with different metal oxide loads were examined for ammoxidation reaction.

Materials and methods

Catalyst preparation

$\text{CrVO}_4/\text{SiO}_2$ catalysts were prepared by spray-drying method. The following precursors were used for the preparation of $\text{CrVO}_4/\text{SiO}_2$ catalysts: V_2O_5 (Aladdin, 99%), CrO_3 (Aladdin, 99%), oxalic acid (Aladdin, 99%), and colloidal silica (Sigma-Aldrich, 30 wt% SiO_2 , 0.6 wt% Na_2O , particle size 16 nm). Appropriate amount of $\text{H}_2\text{C}_2\text{O}_4 \cdot 2\text{H}_2\text{O}$ was dissolved in deionized water. V_2O_5 and CrO_3 with a molar ratio of 1: 2 were added in sequence under vigorous stirring, forming a homogeneous mixture. After adding a certain volume of colloidal silica to the above solution, the resulting mixture was spray-dried at 180 °C in a centrifugal spray dryer. The spray-dried powder was heated at 300 °C for 2 h in a box furnace and then calcined at 550 °C for 4 h. The obtained

CrVO₄/SiO₂ catalysts were labeled as Cat-MO_x, where *x* represents the weight contents of metal oxides in the synthetic catalysts and *x* = 20, 30, 40, 50, 60, 70, and 100%.

The CrVO₄/SiO₂ catalyst with 20% content of metal oxides was prepared for comparison through wetness impregnation method, in which silica was used as support. The obtained catalyst was named as Cat-PTVCrO.

Catalyst characterization

The morphology of Cat-MO_x catalysts was investigated with polarizing microscopy (Polarizing Microscope Axioskop, Zeiss, Germany). The particle size distribution profile was determined with a particle size distribution analyzer (Zetasizer Nano ZS90, Malvern, UK). Powder X-ray diffraction (XRD) patterns were recorded on a Bruker Advanced D8 X-ray diffractometer using Cu K α radiation ($\lambda = 1.54178 \text{ \AA}$) operating at 40 kV and 40 mA. Data were recorded in the range of $2\theta = 10 - 90^\circ$ with a scan step width of 0.0163° . Fourier transform infrared spectra (FT-IR) were measured using a NEXUS470 FT-IR spectrometer (Thermo Nicolet, USA) following the KBr pellet method. Nitrogen adsorption experiments were performed at -196°C using a JW-BK132F gas adsorption analyzer. Before the measurement, the samples were degassed at 200°C for 4 h. X-ray photoelectron spectroscopy (XPS) data were obtained using a MULTILAB2000 X-ray photoelectron spectrometer (VG, USA) with an Al K α X-ray beam as the excitation source. The binding energies (BE) were calibrated against the C 1s peak at 284.6 eV. Temperature-programmed reduction (TPR) experiments were carried out on an AMI-200 Catalyst Multifunctional Characterization Analyzer (Zeton Altimira, USA).

Catalytic performance

Chlorotoluene ammoxidation runs were performed in a fixed-bed reactor, which was made of a Pyrex glass tube (about 500 mm in length and 30 mm in inner diameter). The tube was heated in an electric furnace. About 20 g of catalyst was loaded in the middle of the tube reactor. Both NH₃ and air were quantified using gas flow meters. Chlorotoluenes were injected into a vaporizer through a micropump, mixed with air and NH₃, and then fed into the reactor. The product was collected behind the reactor and was dissolved in ethanol. All the soluble products and unconverted reactants were analyzed by a Shimadzu GC-2010 Plus gas chromatography using a capillary column and an FID detector. A PEG-20 M capillary column (15 m \times 0.25 mm, i.d., 0.25 mm film thickness, Lanzhou Atech Technologies Co. Ltd. China) was employed for separation. All the analysis were conducted under the following conditions: N₂ (99.999%) was used as carrier gas, injection port, the capillary column, and the detector at 250, 80, and 270 $^\circ\text{C}$, respectively. The conversion of para-chlorotoluene (PCT), the yield and selectivity of para-chlorobenzonitrile (PCBN) could be determined by:

$$\text{PCT Conversion(\%)} = \left[1 - n(\text{PCT})_{\text{outlet}} / n(\text{PCT})_{\text{inlet}} \right] \times 100 \quad (1)$$

$$\text{PCBN Molar Yield}(\%) = \left[n(\text{PCBN})_{\text{obtained}} / n(\text{PCT})_{\text{inlet}} \right] \times 100 \quad (2)$$

$$\text{PCBN Selectivity}(\%) = \left[\text{Conversion} / \text{Molar } E \right] \times 100 \quad (3)$$

Results and discussion

Optical microscope

The size and morphology of Cat-MO_x particles were witnessed via an optical microscope. The magnification was 200× and the scale length was 100 μm. Light micrographs of Cat-MO_x particles are shown in Fig. 1. Cat-MO_x particles were well dispersed, and no significant aggregations were observed. The particles had spherical shape in the size range from 20 to 80 μm. The particle size decreased with the increase of metal oxide content. Precursors with low SiO₂ content comprised high content of oxalates. The precursors with high oxalate content decomposed at high temperature and generated a large amount of gas, leading to the disintegration of spherical particles.

Particle size distribution

The particle size distribution (PSD) profiles of spray-dried Cat-MO_x catalysts with various metal oxide contents were measured, and the results are shown in Fig. 2 and Table 1. The PSD profiles of Cat-MO₂₀, Cat-MO₃₀, and Cat-MO₄₀ samples featured a wide particle size distribution in the range of 20–120 μm. Cat-MO₅₀ and Cat-MO₆₀ samples exhibited a less wide particle size distribution in the range of 20–80 μm. Unsupported Cat-MO₁₀₀ sample had a particle size distribution in the range of 10–50 μm. These results indicated that higher metal oxide content led to narrower particle size distributions and smaller diameters.

The PSD profiles of Cat-PTVCrO catalyst and the colloidal silica support are presented in Fig. 3. Both the PSD profiles had a particle size distribution in the range of 50–300 μm. The catalyst particles prepared by wetness impregnation method had similar PSD with formed silica carrier. This was probably due to the low loading of metal oxides over colloidal silica.

X-ray powder diffraction (XRD)

XRD characterization was performed to check the effect of metal oxide contents on the structure of Cat-MO_x catalysts. The XRD patterns of Cat-MO_x ($x = 20\text{--}100$) samples are shown in Fig. 4 for comparison. The broad peak around $2\theta = 23^\circ$ corresponded to the amorphous structure of SiO₂ support. For the samples of $30 \leq x \leq 70$, the XRD patterns agreed well with PDF#51-0031, which corresponded to *monoclinic* CrVO₄ [26], and no diffraction peaks of impurity could be observed. The intensities of XRD peaks gradually increased with the increase of x . It was also

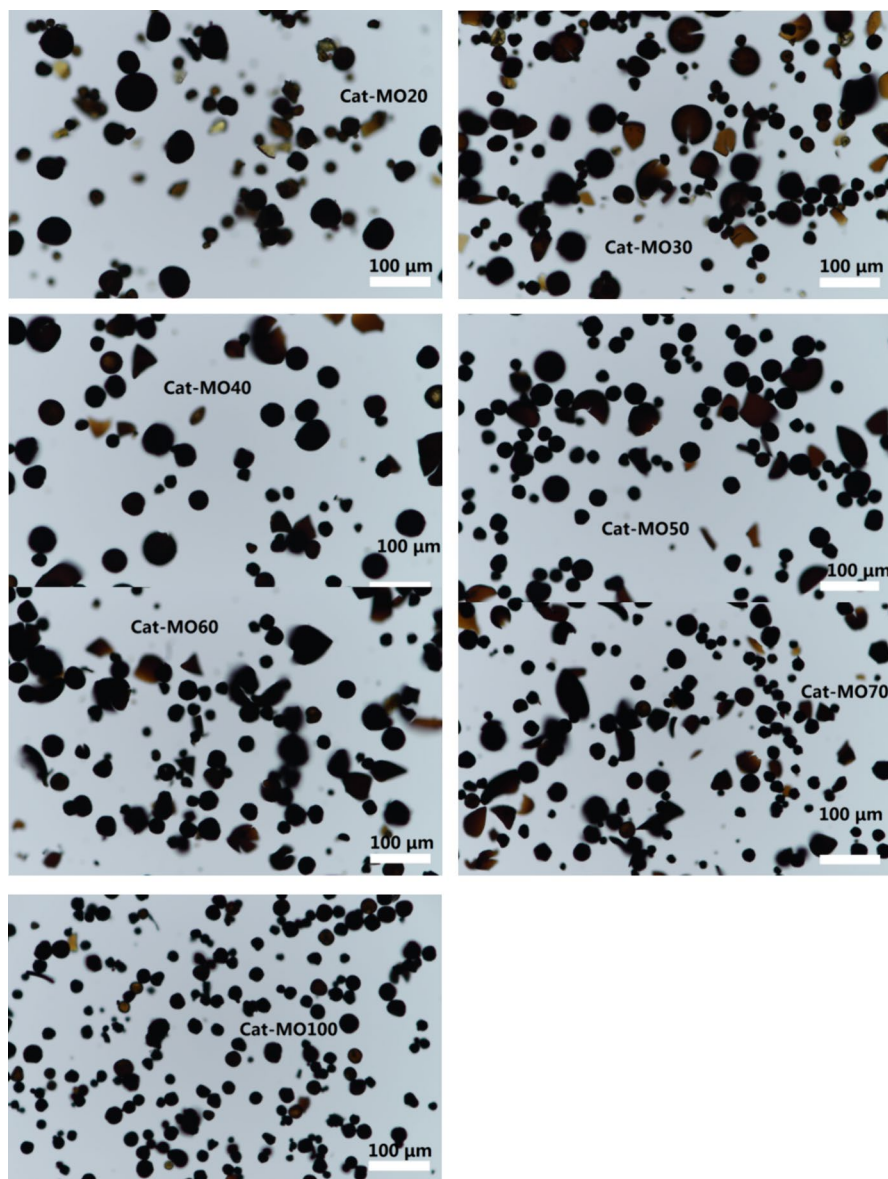


Fig. 1 Light micrographs of Cat-MO x ($x=20, 30, 40, 50, 60, 70,$ and 100) catalysts

found that Cat-MO20 and Cat-MO100 samples were indexed to be dominant *monoclinic* CrVO $_4$ (PDF#51-0031) phase. For the Cat-MO20 sample, diffraction peaks for *hexagonal*-Cr $_2$ O $_3$ (PDF#38-1479) phase were traced, suggested that in the low loading catalyst, the interaction between metal oxide specimen and the silica support could hinder the formation of CrVO $_4$ phase and promote the formation of amorphous V $^{5+}$ phase and Cr $_2$ O $_3$ phase. On the high loading sample, however, the

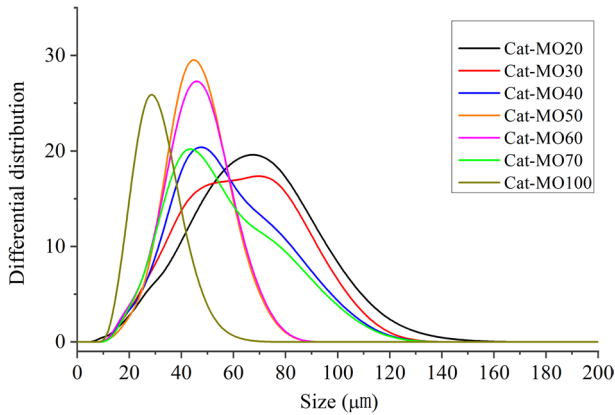


Fig. 2 Particle size distribution of catalysts with different metal oxide contents

Table 1 Particle size characteristics of catalysts with different metal oxide contents

Cat-MO _x	MO20	MO30	MO40	MO50	MO60	MO70	MO100
D50/μm	51.61	46.84	42.70	38.41	38.11	40.04	24.87

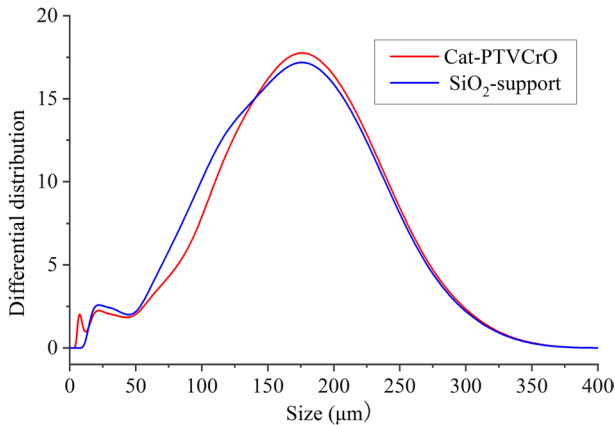


Fig. 3 Particle size distribution of Cat-PTVCrO catalyst and the colloidal silica support

metal oxide species could easily be precipitated next to the silica surface and be aggregated together with the *monoclinic* CrVO_4 phase, due to the relatively weak interaction with the silica support. Compared with standard card of *monoclinic* CrVO_4 , the XRD pattern of Cat-MO100 appeared weak miscellaneous peaks around 24.296° , 26.223° , 32.053° , 35.684° , 36.440° , and 64.171° , which could be ascribed to *orthorhombic* CrVO_4 (PDF#38-1376). For the Cat-PTVCrO sample, the possible CrVO_4 phase was not formed, and instead, only the *hexagonal*- Cr_2O_3 phase

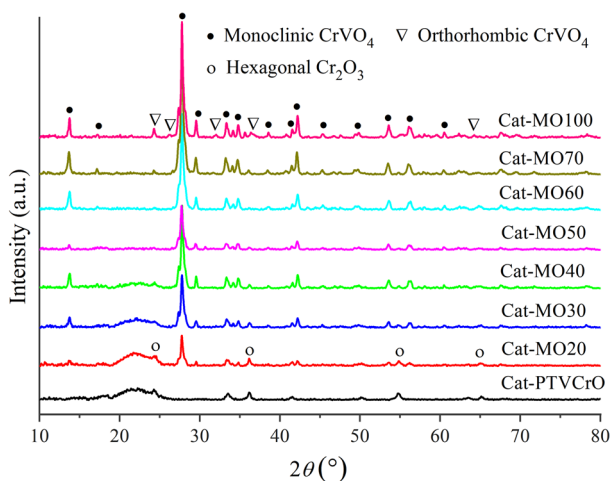


Fig. 4 Powder XRD patterns of Cat-MO $_x$ ($x=20$ – 100) and Cat-PTVCrO

appeared. Cat-PTVCrO was prepared via an incipient wetness impregnation method with a low vanadium-chromium loading. This result suggested that the supported V–Cr–O component was mostly in amorphous form.

Fourier transform IR spectra (FT-IR)

FT-IR spectroscopy was used to verify the change in the skeletal structures of SiO₂ resulting from loading the metal oxides. The FT-IR spectra of Cat-MO $_x$ ($x=20$, 50, and 60) samples are shown in Fig. 5. In the fingerprint region, there are one absorption band at 956 cm⁻¹ attributed to V⁵⁺=O bond stretching, two absorption bands at 869 and 548 cm⁻¹ assigned to V–O–V bending vibration and stretching vibration,

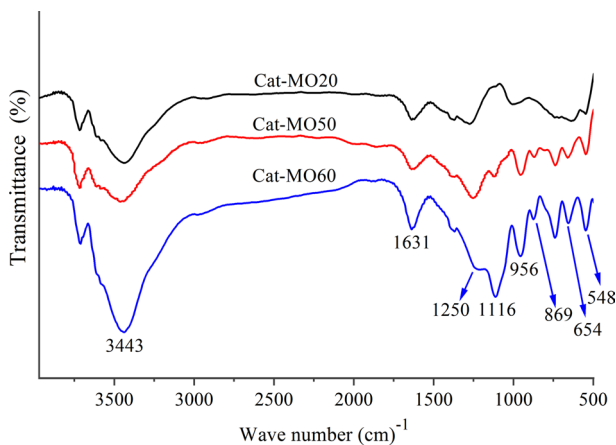


Fig. 5 FT-IR spectra of Cat-MO $_x$ ($x=20$, 50, 60) samples

and two bands at 1250 and 654 cm^{-1} due to the vibrations of Cr–O–Cr and Cr–O. The band peaked at 1116 cm^{-1} was related to the antisymmetric stretching vibration of Si–O–Si [30], suggesting that the skeletal structures of SiO_2 were not damaged as the metal oxides were loaded.

X-ray photoelectron spectroscopy (XPS)

The XPS analysis was carried out to elucidate the chemical states of V, Cr, and O presented in the surface region of Cat-MO x ($x=20\text{--}100$) samples. The survey XPS spectrum of the Cat-MO50 sample contained the Cr, V, O, Si, and C peaks (Fig. 6a). The C 1s peak was originated from the organic residues of the XPS instrument itself. The high-resolution Cr 2p spectrum (Fig. 6b) was resolved into two peaks located at 576.6 and 586.6 eV, assigning to the binding energies of Cr 2p 3/2 and Cr 2p 1/2 [31]. The V 2p spectrum (Fig. 6c) exhibits two peaks at 516.6 and 523.2 eV (V 2p1/2 and V 2p3/2) ascribed predominantly to V^{5+} oxidation state [32]. Additionally, the O 1s peak could be attributed to the oxygen bonds with Cr or V in the CrVO_4 lattice.

The high-resolution XPS spectra of Cr and V + O regions are presented in Fig. 7a and b, respectively. The detailed results are summarized in Table 2. The binding energies (BE) of Cr 2p, V 2p, and O 1s showed no appreciable differences when

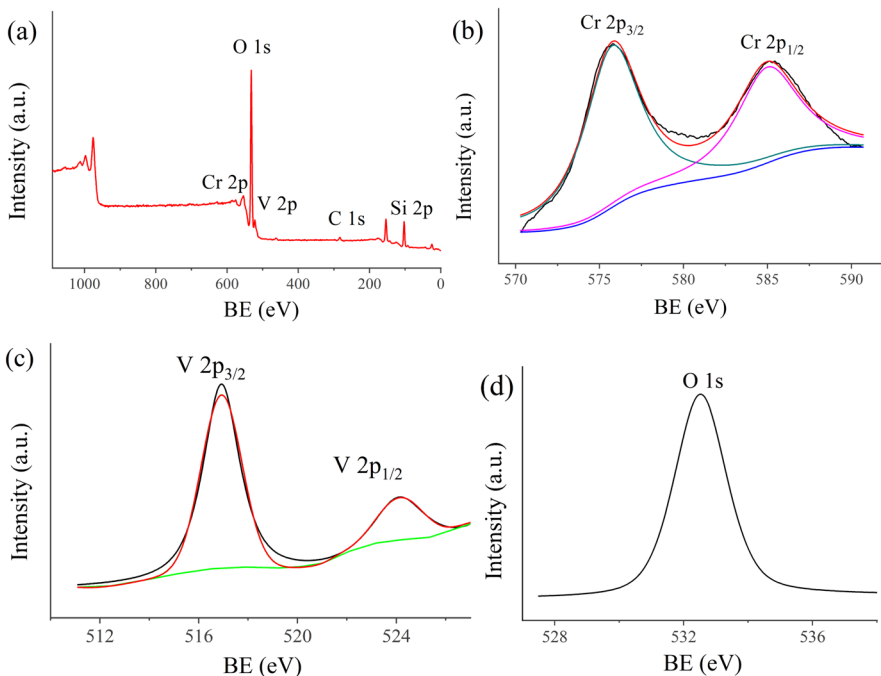


Fig. 6 Full XPS spectrum of Cat-MO60 (a); Cr 2p_{3/2} and Cr 2p_{1/2} XPS spectrum (b); V 2p_{3/2} and V 2p_{1/2} XPS spectrum (c); O 1s XPS spectrum (d)

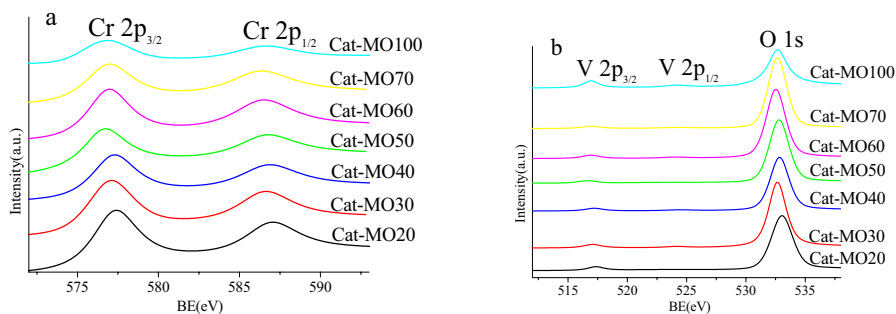


Fig. 7 High-resolution XPS spectra of Cr 2p (a), V 2p and O 1s (b) for the Cat-MO_x catalysts with different metal oxide contents (*x*)

Table 2 XPS results of the Cat-MO_x (*x*=20–100) samples

MO content	20%	30%	40%	50%	60%	70%	100%
Sample	MO20	MO30	MO40	MO50	MO60	MO70	MO100
V 2p _{3/2}	517.4	517.1	517.2	516.6	516.9	516.9	516.9
V 2p _{1/2}	523.1	524.1	524.4	523.2	524.1	524.2	524.1
O 1s	533.0	532.7	532.8	532.8	532.5	532.7	532.7
Cr 2p _{3/2}	577.3	577.0	577.2	576.6	576.9	576.9	576.7
Cr 2p _{1/2}	587.0	586.5	586.8	586.6	586.4	586.3	586.5
Ratio of Cr/V	0.96:1	1:1	0.90:1	1.14:1	1:1	1.20:1	2.13:1

the metal oxide content was raised from 20 to 100%. The results suggested that oxidation states of Cr and V remained constant. Meanwhile, the surface atomic Cr/V ratios were close to 1:1, which was the nominal value of Cr/V molar ratio in CrVO₄, suggesting a well dispersion of metal oxides on the surface of catalysts.

BET surface area

BET gas sorptometry measurement was used to investigate the surface area and the porosity nature of Cat-MO_x samples. The N₂ adsorption–desorption isotherms for the Cat-MO_x (*x*=20, 50, 60, 100) samples are presented in Fig. 8. The data of BET surface area, the average pore volume, and size are given in Table 3. The N₂ adsorption–desorption isotherms for Cat-MO_x samples displayed a type-IV hysteresis loop, characteristic of micro/mesoporous materials [33]. As shown in Table 3, the surface area of the unsupported catalyst (Cat-MO100) was 18.123 m²g⁻¹ and the pore volume was 0.079 cm³ g⁻¹, which were much lower than that of supported Cat-MO_x (*x*=20, 50, 60) samples. The surface area and pore volume of supported catalyst increased firstly, reached the highest values of 73.574 m²g⁻¹ and 0.267 cm³ g⁻¹ at *x*=0.50, and then decreased with increasing CrVO₄ loading from *x*=20 to 60. However, the

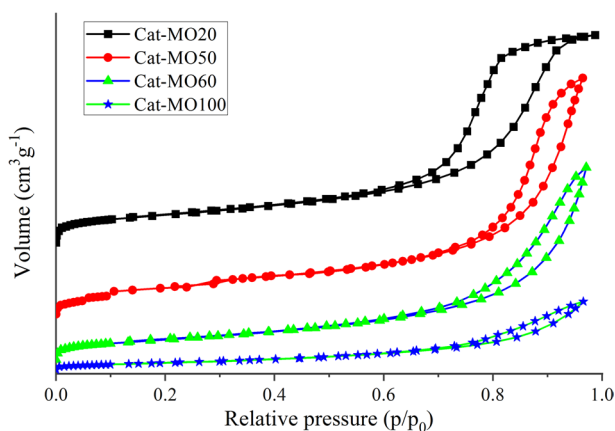


Fig. 8 Nitrogen adsorption–desorption isotherms of Cat-MO $_x$ ($x = 20, 50, 60, 100$)

Table 3 Pore structure parameters of Cat-MO $_x$ catalyst

Sample	Specific surface (m^2g^{-1})	Pore volume (cm^3g^{-1})	Pore size (nm)
Cat-MO20	66.893	0.244	8.324
Cat-MO50	73.574	0.267	10.383
Cat-MO60	50.612	0.214	11.075
Cat-MO100	18.123	0.079	9.437

pore size was increased continuously from 8.324 to 11.075 nm, as displayed in Table 3. The loaded CrVO_4 species could plug the pore mouth, resulting in those pores inaccessible for N_2 adsorption and consequently a decrease in the surface area and pore volume. Moreover, some larger pores were formed on the higher loading Cat-MO $_x$ sample, due probably to the generation of large volume gas products during thermal decomposition of the oxalate precursor at high temperature. Thus, the contents of SiO_2 support and oxalate precursor jointly determined the surface area and porosity of Cat-MO $_x$ sample.

H_2 -TPR

The H_2 -TPR profiles of Cat-MO $_x$ ($x = 20$ – 100) samples are shown in Fig. 9. Pure Cat-MO100 showed one H_2 consumption peak at ~ 442 °C, which corresponded to the reduction of V^{5+} to V^{3+} [34, 35]. The additional SiO_2 support significantly modified the reduction profiles and caused a shift in the main reduction peak to higher temperatures, which was certainly due to the interaction between the metal oxides and the SiO_2 support.

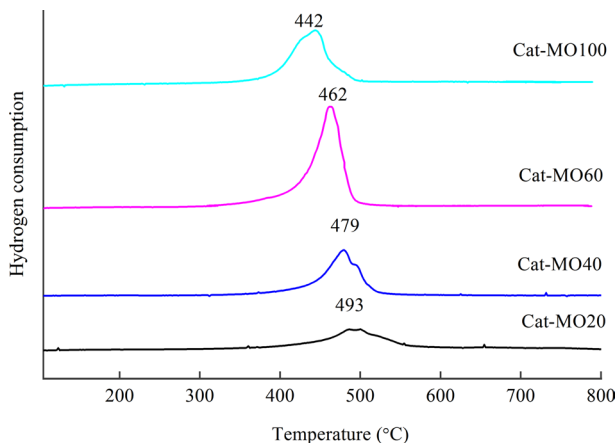


Fig. 9 TPR of Cat-MO x ($x=20, 40, 60, 100$) samples

Catalyst activity

Activities of Cat-MO x catalysts were investigated for the vapor-phase ammoxidation of PCT to PCBN. All the reaction conditions including reaction temperature, $n(\text{NH}_3)/n(\text{PCT})$, $n(\text{air})/n(\text{PCT})$, and loading of metal oxides were assessed in the ammoxidation of PCT over Cat-MO60 catalyst. The influence of reaction temperature on the activity, selectivity, and yield behavior of Cat-MO60 catalysts is shown in Fig. 10a. It was observed that the conversion of PCT increased from 98.5% to almost 100% upon a temperature increase from 380 to 420 °C. The selectivity and yield of PCBN were increased initially and then remained constant upon an increase in the temperature. The maximum selectivity and yield of PCBN observed at 410 °C were 87.61% and 87.38%, respectively. The selectivity and yield of PCBN decreased at the reaction temperature higher than 410°C due to the thermal decomposition or deep oxidation of PCBN.

As shown in Fig. 10b, the molar ratio of $n(\text{NH}_3)/n(\text{PCT})$ had a pronounced promotion effect on the ammoxidation of PCT. As the $n(\text{NH}_3)/n(\text{PCT})$ ratio increased from 1 to 3, the conversion of PCT increased initially and then reached maximum at around 99.5%. The selectivity and yield of PCBN had the same trend. On the surface of Cat-MO60 catalyst, increasing the NH_3 content led to an increase of $M=\text{NH}$ species, which were formed via the condensation reaction between terminal $M=\text{O}$ with NH_3 along with the loss of water [36]. Further increase in the NH_3 content led to a reduction of the O_2 supply and a decrease in the yield and selectivity.

The evolution of catalytic behavior as a function of the $n(\text{air})/n(\text{PCT})$ ratio in the range of 11–21 is shown in Fig. 10c. The conversion of PCT kept constant with increasing the $n(\text{air})/n(\text{PCT})$ ratio, while the selectivity and yield of PCBN increased firstly to a maximum at 15 and then decreased. Obviously, high $n(\text{air})/n(\text{PCT})$ ratio was benefit from the recovery of lattice oxygen. However, excess oxygen content might lead to the deep oxidation of PCBN.

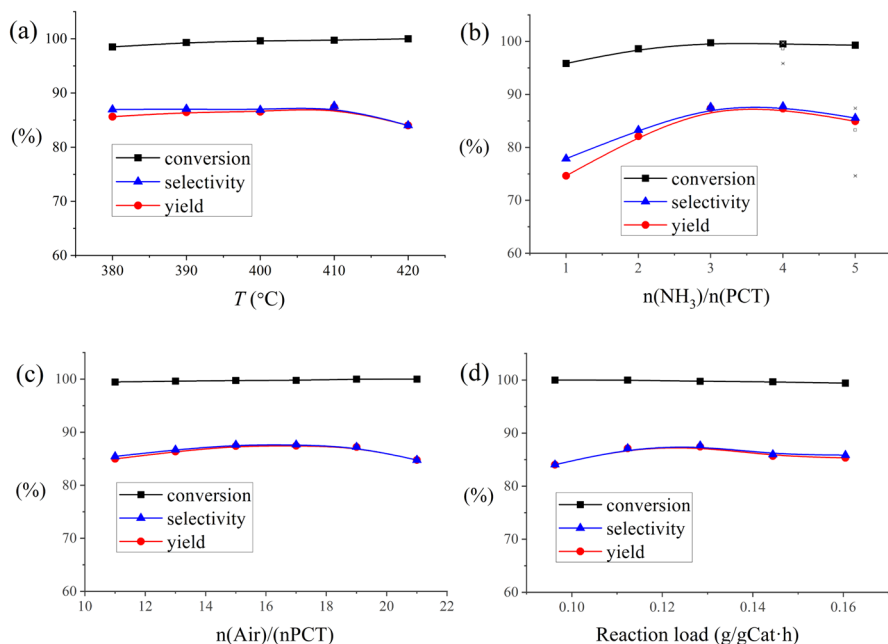


Fig. 10 Effects of reaction parameters on the performance of Cat-MO60 catalyst: **a** Reaction load: 0.13 g/gCat-h; $n(\text{NH}_3)/n(\text{PCT})=1:3$; $n(\text{air})/n(\text{PCT})=15$. **b** $T=410^\circ\text{C}$; reaction load: 0.13 g/gCat-h; $n(\text{air})/n(\text{PCT})=15$. **c** $T=410^\circ\text{C}$; Reaction load: 0.13 g/gCat-h; $n(\text{NH}_3)/n(\text{PCT})=1:3$. **d** $T=410^\circ\text{C}$; $n(\text{NH}_3)/n(\text{PCT})=1:3$; $n(\text{air})/n(\text{PCT})=15$

The effect of reaction load over Cat-MO60 catalyst bed was studied, and the results are shown in Fig. 10d. With an increase in the reaction load, the conversion of PCT slightly decreased due to a reduction in contact time between the reactant and active sites. Lower reaction load prolonged the contact time, leading to somewhat lower yield and selectivity due to the deep oxidation of PCBN over the catalyst. The best yield and selectivity were obtained at a reaction load of 0.13 g/gCat-h.

As discussed above, the optimal reaction conditions could be determined as follows: $T=410^\circ\text{C}$, $n(\text{PCT}):n(\text{NH}_3):n(\text{air})=1:3:15$; reaction load=0.13 g/gCat-h. The activity of Cat-MO_x catalysts for the ammoxidation of PCT was evaluated. During the ammoxidation of PCT over these catalysts, PCBN was the desired product and other possible by products, such as benzonitrile, chlorobenzene, and toluene, were not detected. The variation in the catalytic activity was observed with change in the CrVO₄ loading in the catalysts, and the results are depicted in Fig. 11. The Cat-MO20 catalyst exhibited only 57.14% conversion of PCT and 43.55% yield of PCBN. When the metal oxides loading increased up to 60 wt%, the conversion of PCT and the yield of PCBN increased up to 99.62% and 86.52%, respectively. However, for Cat-MO100 catalyst, which contains no SiO₂ support, the conversion of PCT and the yield of PCBN were with levels of 98.62% and 78.30%, respectively.

Since silica support showed no catalytic activity under the same experimental conditions, the performance measured should be merely attributed to the supported

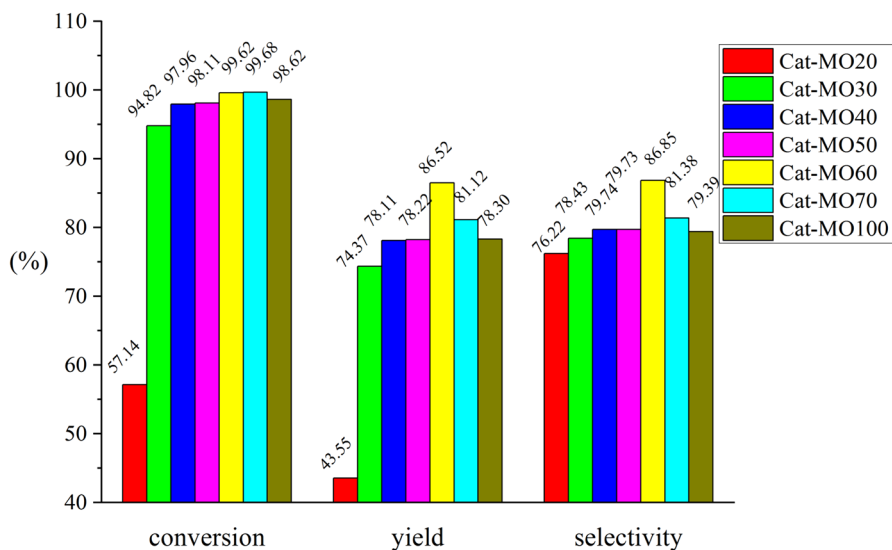


Fig. 11 Activity of Cat-MO_x catalysts for PCT ammoxidation at: $T=410$ °C; reaction load: 0.13 g/gCat-h; $n(\text{NH}_3)/n(\text{PCT})=1:3$; $n(\text{air})/n(\text{PCT})=15$

CrVO₄ species. Generally, Cat-MO100 showed lower activity than the supported catalyst. The inner CrVO₄ species was not accessible in the bulk phase of CrVO₄. If the CrVO₄ phase was dispersed on the support with high surface area, more active species exposed and the number of available reactive sites increased. On the contrary, in samples supported with high level of SiO₂, CrVO₄ species could be heavily embedded and only a small amount of CrVO₄ species exposed on the surface due to active components and carrier silica dispersed almost uniformly on the surface and inner of catalysts, leading to a decrease of the catalytic activity. As displayed in Fig. 11, the Cat-MO60 catalyst showed the highest PCT conversion and PCBN yield in comparison with the other supported or pure catalysts.

The performance of Cat-PTVCrO catalyst was also tested in the same conditions for comparison, and the results are depicted in Fig. 12. Although the conversion of PCT was close to 100%, both the selectivity and yield of PCBN were obviously below than those obtained over Cat-MO60 catalyst. Furthermore, the reaction load was quite low. All these results suggested that the spray-drying technique showed significant advantages in preparing ammoxidation catalysts.

In addition, the catalytic behavior of the Cat-MO60 catalyst was also investigated in the ammoxidation reaction of toluene and other chloro-substituted toluenes such as meta-chlorotoluene (MCT) and ortho-chlorotoluene (OCT), and the results are depicted in Fig. 13 and Table 4. Cat-MO60 catalyst exhibited equally excellent catalytic ability in these reactions. The catalytic behaviors of some reported catalysts are also listed in Table 4. It was obvious that Cat-MO60 catalyst showed improved catalytic performances among the previous reported composite oxide catalysts.

Meanwhile, the position of Cl group had an obvious influence on the catalytic activity of ammoxidation reaction. The Cl group had a weak electron-withdrawing

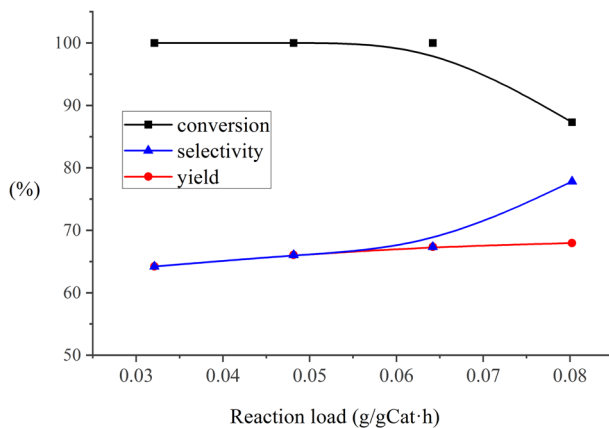


Fig. 12 Activity of Cat-PTVCrO catalysts for PCT ammoxidation

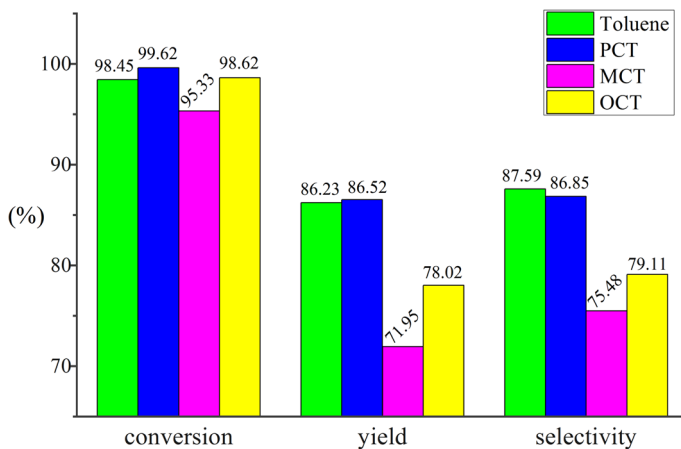


Fig. 13 Catalytic activities of Cat-MO60 in the ammoxidation of toluene, PCT, MCT, and OCT

Table 4 Comparison for the ammoxidation of PCT and OCT

Substrate	Catalyst	T ($^{\circ}\text{C}$)	Conversion (%)	Yield (%)	Selectivity (%)	Refs.
PCT	Cat-MO60	410	99.6	86.5	86.8	This work
OCT	Cat-MO60	410	98.6	78.0	79.1	This work
PCT	MoV_2O_8	440	99.6	83.6	83.9	[12]
PCT	Bulk-VPO	410	98	93	95	[37]
PCT	Nano- $\text{Cr}_2\text{V}_4\text{O}_{13}$	390	97.8	89.7	91.7	[9]
OCT	Nano- $\text{Cr}_2\text{V}_4\text{O}_{13}$	410	85.4	74.9	87.7	[9]
OCT	Nano- CrVO_4	410	94.1	81.7	86.8	[10]
OCT	Bulk-VPO	430	70	50	71	[38]

effect. The accessibility and reactivity of $-CH_3$ group are dependent on the position of $-Cl$ group. The Cl group in para position had almost no steric hindrance in activating the methyl group. For PCT the process got the highest conversion of PCT and yield of PCBN, but the selectivity was slightly lower than that for toluene due to the deep oxidation of PCBN at high temperature. OCT had the electronic similarity with PCT but more steric hindrance, leading to obviously lower activity. Due to the serious electron-withdrawing effect of Cl substituent in the meta-position, the ammoxidation process exhibited the lowest conversion of MCT and the lowest yield and selectivity of meta-chlorobenzonitrile (MCBN). These results were consistent with that reported previously [37, 39].

Conclusions

We synthesized $CrVO_4/SiO_2$ catalysts with different metal oxides content, characterized their physicochemical properties, and conducted ammoxidation reactions. The catalysts were synthesized by spray-drying method, i.e., wet mixing Cr and V precursors with colloidal silica, spray drying the mixture, and calcining at $550\text{ }^\circ\text{C}$ for 4 h. The spray-dried $CrVO_4/SiO_2$ microspheres were highly dispersed with diameter about $20\text{--}80\text{ }\mu\text{m}$. The as-synthesized $CrVO_4/SiO_2$ catalysts showed the same *monoclinic* $CrVO_4$ phase as the weight contents of metal oxides located in the range of 30%–70%. Among them, $CrVO_4/SiO_2$ catalysts with metal oxides of 60% exhibited the best performance in PCT ammoxidation reaction. This study may pave the way for the large-scale preparation of supported catalysts used in the vapor-phase ammoxidation reactions.

Author contributions All authors contributed to the study conception and design. Material preparation, data collection, and analysis were performed by Jiale Tong and Y. Huang. The first draft of the manuscript was written and revised by W. Tang. The manuscript was revised by Q. You, and all authors commented on previous versions of the manuscript. G. Xie did project administration, supervised the work, revised, and completed the manuscript. All authors read and approved the final manuscript.

Funding This work was supported by the National Natural Science Foundation of China (Grant No. 21172269), the Fundamental Research Funds for the Central Universities, South-Central Minzu University (Grant No. CZY22010), the Major bidding projects of provincial and ministerial scientific institutions, South-Central Minzu University (Grant No. PTZD22007), and the Opening Project of Key Laboratory of Optoelectronic Chemical Materials and Devices of Ministry of Education, Jiangnan University (Grant No. JDGD-202220).

Data availability The data and materials can be accessed from the manuscript for the current study.

Declarations

Conflict of interest The authors declare that they have no known competing financial interests or personal relationships that could have appeared to influence the work reported in this paper.

Ethical approval Not applicable.

References

1. K.S. Akers, G.D. Sinks, T.W. Schultz, *Environ. Toxicol. Phar.* **7**(1), 33 (1999)
2. B.S. Bahl, A. Bhal, *Advanced organic chemistry*, 4th edn, (S. Chand and Company Ltd., 1995) p. 1117
3. A. Martin, V.N. Kalevaru, *ChemCatChem* **2**, 1504 (2010)
4. M. Faizan, R. Zhang, R. Liu, *J. Ind. Eng. Chem.* **110**, 27 (2022)
5. S.K. Sharma, A. Kumar, G. Sharma, M. Naushad, D.-V.N. Vo, M. Alam, F.J. Stadler, *Mater. Lett.* **281**, 128650 (2020)
6. M. Touboul, K. Melghit, *J Mater Chem* **5**(1), 147 (1995)
7. L. Xu, Y. Zhang, Y. Deng, Y. Zhong, S. Mo, G. Cheng, C. Huang, *Mater. Res. Bull.* **48**, 3620 (2013)
8. Y. Liu, D. Zhao, W. Tang, T. Li, Q. You, G. Xie, *Catal. Lett.* **154**, 524 (2024)
9. W. Tang, H. Zheng, Y. Dong, Q. You, T. Li, G. Xie, *Mol. Catal.* **518**, 112062 (2022)
10. Y. Huang, T. Li, Q. You, X. You, Q. Zhang, D. Zhang, G. Xie, *Chin. J. Catal.* **39**, 1814 (2018)
11. D. Zhao, W. Tang, Q. You, T. Li, L. Sun, G. Xie, *Res. Chem. Intermed.* **49**, 4367 (2023)
12. W. Tang, Y. Liu, S. Ding, D. Zhao, T. Li, G. Xie, *Res. Chem. Intermed.* **48**, 4105 (2022)
13. Y. Dong, T. Li, X. You, Q. You, L. Sun, G. Xie, *Res. Chem. Intermed.* **48**, 1151 (2022)
14. G. Xie, A. Zhang, *Synth. Commun.* **42**, 375 (2012)
15. G. Xie, A. Zhang, C. Huang, *Res. Chem. Intermed.* **36**, 969 (2010)
16. T. Tabanelli, M. Mari, F. Folco, F. Tanganelli, F. Puzzo, L. Setti, F. Cavani, *Appl. Catal. A* **619**, 118139 (2021)
17. I. Zbicinski, A. Delag, C. Strumillo, J. Adamiec, *Chem. Eng. J.* **86**, 207 (2002)
18. T. Shoinkhorova, A. Dikhtiarenko, A. Ramirez, A.D. Chowdhury, M. Caglayan, J. Vittenet, A. Bendjeriou-Sedjerari, O.S. Ali, I. Morales-Osorio, W. Xu, J. Gascon, *A.C.S. Appl. Mater. Interf.* **11**, 44133 (2019)
19. M. Santiago, A. Restuccia, F. Gramm, J. Perez-Ramírez, *Micropor. Mesopor. Mat.* **146**, 76 (2011)
20. N. Saadatkhah, M.G. Rigamonti, D.C. Boffito, H. Li, G.S. Patience, *Powder Technol.* **316**, 434 (2017)
21. F. Iskandar, I.W. Lenggoro, B. Xia, K. Okuyama, *J. Nanoparticle Res.* **3**, 263 (2001)
22. M. Kim, H.-J. Chae, T.-W. Kim, K.-E. Jeong, C.-U. Kim, S.-Y. Jeong, *J. Ind. Eng. Chem.* **17**, 621 (2011)
23. R. Zhao, J.G. Goodwin Jr., K. Jothimurugesan, S.K. Gangwal, J.J. Spivey, *Ind. Eng. Chem. Res.* **40**, 1320 (2001)
24. F. Iskandar, L. Gradon, K. Okuyama, *J. Colloid. Interf. Sci.* **265**, 296 (2003)
25. D.-L. Yang, R.-K. Liu, Y. Wei, Q. Sun, J.-X. Wang, *Particuology* **85**, 22 (2024)
26. C. Du, Y. Huang, W. Tang, L. Sun, Q. You, T. Li, G. Xie, *Res. Chem. Intermed.* **49**, 5361 (2023)
27. V.N. Kalevaru, N. Madaan, A. Martin, *Appl. Catal. A* **391**(1), 52 (2011)
28. P. Borah, A. Ramesh, A. Datta, *Catal. Commun.* **12**(2), 110 (2010)
29. K.V. Narayana, B.D. Raju, S.K. Masthan, V.V. Rao, P.K. Rao, A. Martin, *J. Mol. Catal. A* **223**(1–2), 321 (2004)
30. M.A. Vicente-Rodriguez, M. Suarez, M.A. Bafiares-Mufioz, J. de Dios Lopez-Gonzalez, *Spectrochim. Acta A* **52**, 1685 (1996)
31. X. Wang, E. Suhr, L. Banko, S. Salomon, A. Ludwig, *A.C.S. Appl. Electron. Mater.* **2**(4), 1176 (2020)
32. R. Vidruk, M.V. Landau, M. Herskowitz, V. Ezersky, A. Goldbourt, *J. Catal.* **282**, 215 (2011)
33. M.K. And, M. Jaroniec, *Chem. Mater.* **13**, 3169 (2001)
34. S.K. Perumal, H. Yu, P. Aghalayam, H.S. Kim, *Energy Fuels* **38**(5), 4516 (2024)
35. S.K. Perumal, U. Samidurai, V.G. Balashanmugam, H.S. Kim, P. Aghalayam, *Sep. Purif. Technol.* **322**, 124181 (2023)
36. R.K. Grasselli, J.D. Burrington, D.J. Buttrey, *Top. Catal.* **23**(1–4), 5 (2003)
37. A. Martin, B. Lücke, *Catal. Today* **32**, 279 (1996)
38. A. Martin, B. Lücke, G. Wolf, M. Meisel, *Catal. Lett.* **33**, 349 (1995)
39. G. Xie, C. Huang, *Indian J. Chem. Technol.* **14**, 371 (2007)

Publisher's Note Springer Nature remains neutral with regard to jurisdictional claims in published maps and institutional affiliations.

Springer Nature or its licensor (e.g. a society or other partner) holds exclusive rights to this article under a publishing agreement with the author(s) or other rightsholder(s); author self-archiving of the accepted manuscript version of this article is solely governed by the terms of such publishing agreement and applicable law.

Authors and Affiliations

Jiale Tong¹ · Yeyin Huang¹ · Wanjun Tang¹ · Qingliang You² · Guangyong Xie¹

✉ Wanjun Tang
tangmailbox@126.com

✉ Guangyong Xie
xiegy@scuec.edu.cn

Jiale Tong
2937497032@qq.com

Yeyin Huang
1026306701@qq.com

Qingliang You
yql1976@126.com

¹ Key Laboratory of Catalysis and Energy Materials Chemistry of Ministry of Education & Hubei Key Laboratory of Catalysis and Materials Science, South-Central Minzu University, Wuhan 430074, China

² Key Laboratory of Optoelectronic Chemical Materials and Devices, Ministry of Education, School of Chemical and Environmental Engineering, Jiangnan University, Wuhan 430056, China